

Spin-orbit torque in MgO/CoFeB/Ta/CoFeB/MgO symmetric structure with interlayer antiferromagnetic coupling

G. Y. Shi,¹ C. H. Wan,² Y. S. Chang,² F. Li,¹ X. J. Zhou,¹ P. X. Zhang,¹ J. W. Cai,^{2,*} X. F. Han,² F. Pan,¹ and C. Song^{1,†}

¹Key Laboratory of Advanced Materials (MOE), School of Materials Science and Engineering, Tsinghua University, Beijing 100084, China

²Beijing National Laboratory for Condensed Matter Physics, Institute of Physics, Chinese Academy of Sciences, Beijing 100190, China

(Received 26 November 2016; revised manuscript received 19 January 2017; published 28 March 2017)

Spin current generated by the spin Hall effect in a heavy metal that would diffuse up and down to adjacent ferromagnetic layers and exert torque on their magnetization is called spin-orbit torque. Antiferromagnetically coupled trilayers, namely, the so-called synthetic antiferromagnets usually are employed to serve as the pinned layer of spintronic devices based on spin valves and magnetic tunnel junctions to reduce the stray field and/or increase the pinning field. Here we investigate the spin-orbit torque in a MgO/CoFeB/Ta/CoFeB/MgO perpendicularly magnetized multilayer with interlayer antiferromagnetic coupling. It is found that the magnetization of two CoFeB layers can be switched between two antiparallel states simultaneously. This observation is replicated by the theoretical calculations by solving the Stoner-Wohlfarth model and the Landau-Lifshitz-Gilbert equation. Our findings combine spin-orbit torque and interlayer coupling, which might advance the magnetic memories with a low stray field and low power consumption.

DOI: 10.1103/PhysRevB.95.104435

I. INTRODUCTION

The spin Hall effect (SHE), a robust way to generate spin current, is a transport phenomenon which demonstrates that an electric current flows through nonmagnetic materials and generates orthogonal spin polarization and spin current [1–5]. The efficiency of the charge to spin conversion, characterized by the spin Hall angle, generally depends on the strength of spin-orbit coupling [6–8]. For the in-plane case, up- and down-polarized spins accumulate at the edge of the channel, which was directly detected via the Kerr microscope [3] and Hanle effect [5]. For the out-of-plane case, spins with opposite directions diffuse upward and downward, which exert torques to neighboring magnetic layers. This is the so-called spin-orbit torque (SOT), which is considered as an effective way to switch magnetization [9–19] and to drive domain-wall motion [20,21] with low power consumption. The torque includes two components, e.g., dampinglike torque and fieldlike torque, which have different symmetries with respect to magnetization reversal [22–24]. These torques essentially generated by spin-orbit coupling have also been demonstrated both theoretically and experimentally in antiferromagnetic systems. Gomonay and Loktev [25,26] proposed that dampinglike torque induced by spin-polarized current can produce large-angle reorientation of antiferromagnetic magnetization. And Wadley *et al.* [27] showed the electrical switching of antiferromagnetic CuMnAs via fieldlike torque generated by nonequilibrium spin polarizations. In general, such a system which consists of a heavy metal (HM)/ferromagnetic metal (FM)/oxide heterostructure only utilizes one side of the spin current brought by the SHE. Moreover, Woo *et al.* [28] constructed a Pt/Co/Ta structure to enhance spin-orbit torque due to the opposite sign of the spin Hall angle of Pt and Ta, whereas even in this structure only one side of the spin polarization produced by the SHE of the heavy metals is available for the magnetization switching. Obviously, there

is a pressing need to develop a different structure, e.g., a CoFeB/Ta/CoFeB sandwich, to make use of both spin currents from the Ta layer flowing upward and downward to realize the magnetization switching of two adjacent CoFeB layers.

The interlayer coupling in ferromagnetic/nonmagnetic/ferromagnetic sandwich structures has been studied extensively. It is generally accepted that the coupling oscillates between the ferromagnetic and the antiferromagnetic systems as the nonmagnetic inset layer (such as, Ru and Cr) thickness increases with a long oscillation period of ~ 1 nm, ascribed to the Ruderman-Kittel-Kasuya-Yosida (RKKY) exchange interaction [29–31]. However, the oscillation vanishes, and only antiferromagnetic coupling remains in the sandwich structures with bcc heavy metals, e.g., Nb, Ta, and W [30]. Thus, antiferromagnetic interlayer coupling is expected to play an important role in the SOT-induced magnetization switching in CoFeB/Ta/CoFeB-based heterostructures. The theories and experiments below demonstrate that in perpendicularly magnetized MgO/CoFeB/Ta/CoFeB/MgO heterostructures the two CoFeB layers with antiferromagnetic coupling can be switched between two antiparallel states simultaneously through the SOT.

II. METHOD

MgO(4)/Co₄₀Fe₄₀B₂₀(1.3)/Ta(1.2)/Co₄₀Fe₄₀B₂₀(1.05)/MgO(2)/SiO₂(2) (from the bottom to the top, thickness in nanometers) heterostructures were deposited on thermally oxidized Si substrates via magnetron sputtering at a base vacuum of 5×10^{-5} Pa. In order to optimize the perpendicular magnetic anisotropy (PMA), the films were annealed at 300 °C for half an hour at the vacuum. After that, typical Hall bar devices with channel widths of $3 \mu\text{m}$ were fabricated by lithography and Ar-ion etching. For theoretical calculations, the Stoner-Wohlfarth model [32], torque balance equation, and the Landau-Lifshitz-Gilbert (LLG) equation [10] were adopted to simulate the current-induced magnetization switching in the heterostructures with PMA and antiferromagnetic coupling.

*jwcai@iop.ac.cn

†songcheng@mail.tsinghua.edu.cn

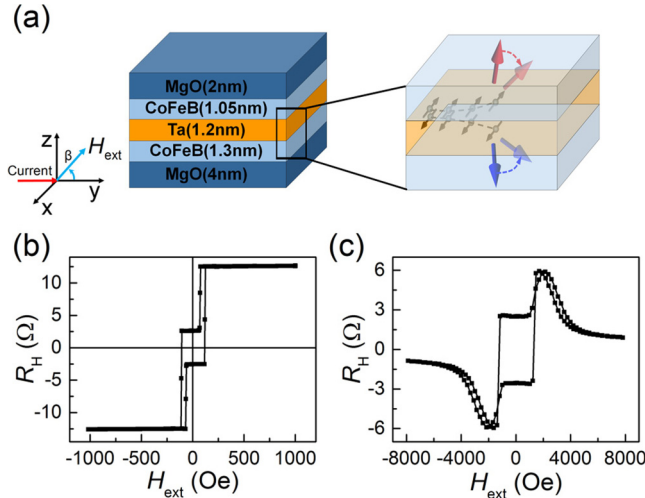


FIG. 1. (a) Schematic of a MgO/CoFeB/Ta/CoFeB/MgO multilayer. The expanded area shows the SHE brought on spin polarization and in turn magnetization switching. R_H curves measured when (b) H_{ext} is fixed in the $+z$ direction and (c) H_{ext} is on the yz plane and near the $+y$ direction ($\beta = 1^\circ$).

III. RESULTS AND DISCUSSION

A. Experiment

Figure 1(a) displays a schematic of the sample layout and measurement configuration. The expanded area exhibits the concept that with the current applied to the Ta layer, and the SHE creates inverse spin polarization, which diffuses up and down into the adjacent CoFeB layers, giving rise to magnetization switching. We first show in Fig. 1(b) an anomalous Hall effect (AHE) curve measured with a current (I) of 0.1 mA applied to the Hall bar along the $+y$ direction and an external magnetic field (H_{ext}) along the z direction ($\beta = 90^\circ$). There are two striking features for the AHE curve: (i) separate switching fields for the upper and lower CoFeB layers, i.e., 72 and -110 Oe for the descending branch with a plateau in between, indicating these two CoFeB layers are antiferromagnetically coupled with each other, and a similar interlayer antiferromagnetic coupling is observed in a series of CoFeB/Ta(t)/CoFeB ($t = 1.0, 1.2, 1.4$, and 1.6 nm) without RKKY oscillation, which is consistent with the observation in Co/Ta multilayers [30]; (ii) the square shape of the AHE curve confirms the PMA of the CoFeB layers, which benefits the current-induced magnetization switching via the SOT. Note that it is the z component of the external field leading to the magnetization reversal when H_{ext} is swept on the yz plane and close to the y axis ($\beta = 1^\circ$), and the sudden change in Hall resistance (R_H) occurs at a much larger external field compared to the case of $\beta = 90^\circ$ as presented in Fig. 1(c). When H_{ext} is up to more than 2 kOe, the magnetization of CoFeB gradually is aligned to a near in-plane position. As a consequence, the z component of the total magnetization continuously reduces, causing the decrease in the Hall resistance.

We then focus on the current-induced magnetization switching via the SOT. For these measurements, a constant external field was applied along the y direction, and the Hall resistance was recorded while sweeping the current. The

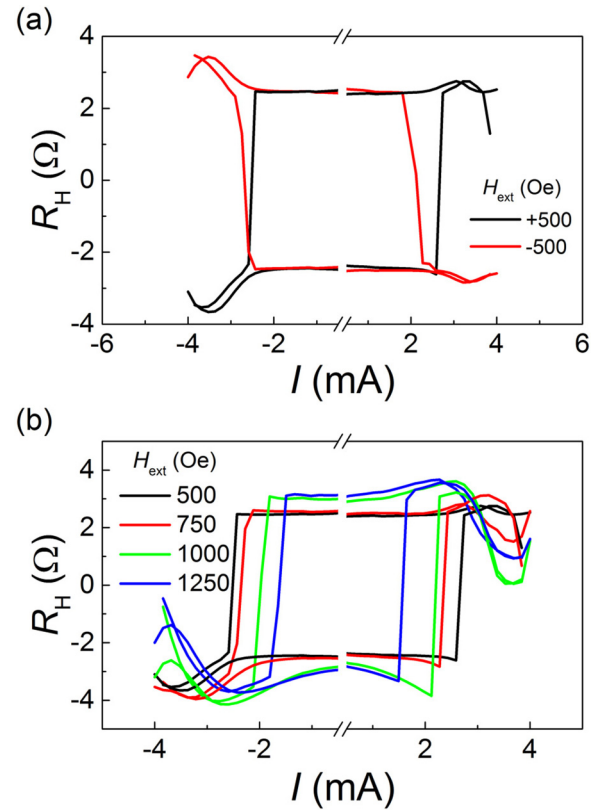


FIG. 2. (a) Magnetization switching characterized by R_H in the presence of positive and negative external fields fixed in the y direction. (b) Current-induced switching under different external magnetic fields applied in the $+y$ direction.

most eminent feature in Fig. 2(a) is that the magnetization switching induced by the current shows a hysteresis window with a critical current of ~ 2.6 mA ($J_e = 2.44 \times 10^7$ A/cm 2) and the switching is anticlockwise for positive H_{ext} ($+500$ Oe) and clockwise for negative H_{ext} (-500 Oe). The switching direction is similar to that of typical Ta/CoFeB/MgO structures [9]. Moreover, the quantity of the Hall resistance at two stable states (± 2.5 Ω) clarifies that the magnetization switching occurs between two antiparallel states of CoFeB moments, which is consistent with the plateau resistance in the AHE curve shown in Fig. 1(b).

A comparison of the current-induced magnetization switching at various external magnetic fields is depicted in Fig. 2(b). Apparently, the critical current for magnetization switching drops with enhancing H_{ext} from 500 to 1250 Oe. Also visible is the gradual decrease in the Hall resistance when the applied current is higher than the critical current. This tendency indicates that the perpendicular magnetized CoFeB would be switched to a position in the vicinity of the yz plane by the strong applied current. Furthermore, when the current is near 4 mA, the Hall resistances suddenly increase due to Joule heating. Particularly, as demonstrated in Fig. 2(b), the current-induced switching curves show the opposite nonlinear behavior at positive and negative values of Hall resistance before the switching. This observation is different from the previous reports in a single ferromagnetic layer system [10,14].

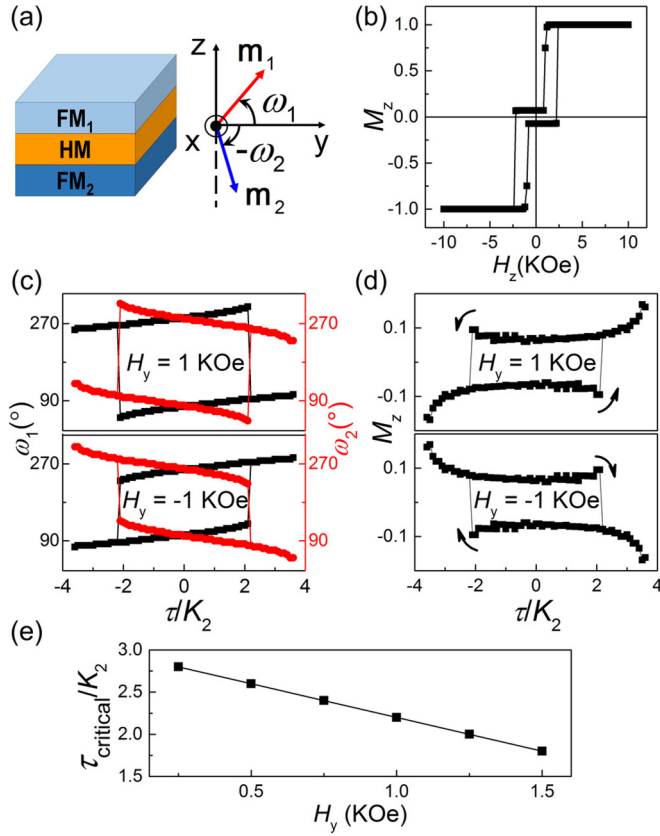


FIG. 3. (a) Sketch of a heavy metal layer sandwiched by two ferromagnetic metal layers and corresponding Cartesian coordinates with relevant orientation of magnetic moments \mathbf{m}_1 and \mathbf{m}_2 . (b) Hysteresis loop calculated by the Stoner-Wohlfarth model. (c) Current-induced switching under positive and negative external fields exhibited by the angular coordinates of \mathbf{m}_1 and \mathbf{m}_2 and (d) the z component of total magnetization M_z . (e) Critical τ for magnetization switching vs the external field by solving the torque balance equation.

B. Simulation

Now, we turn to the simulation part in order to interpret the experimental results. Before utilizing the torque balance equation to simulate current-induced magnetization switching, both the interlayer antiferromagnetic coupling and the PMA features need to be involved with the magnetic state of CoFeB/Ta/CoFeB via the Stoner-Wohlfarth model. On the basis of the Stoner-Wohlfarth model, a simple structure is set up where a heavy metal is sandwiched by two single domain ferromagnetic layers (FM₁ and FM₂) with an easy axis along the z axis as illustrated in Fig. 3(a). While sweeping the external field along the z axis, the hysteresis loop can be obtained by solving the local minimum of free energy of this structure. The free energy consists of Zeeman energy, anisotropy energy, and antiferromagnetic coupling energy,

$$E = -(H_z M_1 \sin \omega_1 + H_z M_2 \sin \omega_2) + K_1 \cos^2 \omega_1 + K_2 \cos^2 \omega_2 + A_{12} \cos(\omega_1 - \omega_2), \quad (1)$$

where M_1 and M_2 are the magnetizations of FM₁ and FM₂, K_1 and K_2 characterize their anisotropy energies, antiferromagnetic coupling energy is expressed by A_{12} , and the angles between the y axis and the magnetization of FM₁ and FM₂

are ω_1 and ω_2 , respectively [Fig. 3(a)]. Considering that the free-energy E is a function of two variables ω_1 and ω_2 , the local minimum of free energy fulfills two conditions: One is

$$\frac{\partial E}{\partial \omega_1} = 0 \quad \text{and} \quad \frac{\partial E}{\partial \omega_2} = 0, \quad (2)$$

and the other is

$$\frac{\partial^2 E}{\partial \omega_1^2} > 0 \quad \text{and} \quad \det \begin{bmatrix} \frac{\partial^2 E}{\partial \omega_1^2} & \frac{\partial^2 E}{\partial \omega_1 \partial \omega_2} \\ \frac{\partial^2 E}{\partial \omega_2 \partial \omega_1} & \frac{\partial^2 E}{\partial \omega_2^2} \end{bmatrix} > 0. \quad (3)$$

Accordingly, the hysteresis loop of the proposed structure could be obtained via solving the specific ω_1 and ω_2 that satisfy Eqs. (2) and (3) for each given external field H_z and bringing them into $M_z = (M_1 \sin \omega_1 + M_2 \sin \omega_2)/(M_1 + M_2)$, which expresses the normalized projection of total magnetization on the z axis. Figure 3(b) shows a representative hysteresis loop by plugging these parameters to Eq. (1): $K_1 = 1.3 \times 10^6$, $K_2 = 1 \times 10^6$, $A_{12} = 2 \times 10^6$ erg/cm³, $M_1 = 1500$, and $M_2 = 1300$ emu/cm³. Remarkably, the shape of the hysteresis loop reflects both the PMA and the antiferromagnetic coupling in the proposed structure.

The static evolution of the magnetization of FM₁ and FM₂ layers can be derived by the torque balance equation [10],

$$\begin{aligned} \tau_{\text{tot}1} &= \tau_{\text{ext}1} + \tau_{\text{an}1} + \tau_{\text{coup}1} - \tau = 0, \\ \tau_{\text{tot}2} &= \tau_{\text{ext}2} + \tau_{\text{an}2} + \tau_{\text{coup}2} + \tau = 0, \end{aligned} \quad (4)$$

where the torques on the magnetic moment including external field torque τ_{ext} , anisotropy field torque τ_{an} , antiferromagnetic coupling field torque τ_{coup} , and spin-orbit torque τ . It is worth pointing out that in the torque balance equation of FM₁ the sign of τ is negative due to the negative spin Hall angle of the HM assumed in the proposed model. Whereas in the torque balance equation of FM₂, the sign of τ is positive considering that the spin polarization induced by the SHE is opposite for spins moving to two opposite directions. For clarity, the scalar expression of torque balance equation for FM₁ and FM₂ is derived from the vector form in Eq. (4) (see Appendix A for the detailed derivation process). The magnetic parameters adopted in Eq. (4) are identical to that of Eq. (1) and the corresponding results are presented in Figs. 3(c) and 3(d). The magnetic moments \mathbf{m}_1 and \mathbf{m}_2 can be rotated on the yz plane and switched simultaneously for a certain amount of τ .

As Fig. 3(c) shows, the z components of \mathbf{m}_1 and \mathbf{m}_2 remain opposite due to the antiferromagnetic coupling in the whole process. Moreover, for a positive external field (e.g., $H_y = 1000$ Oe) and a positive current, \mathbf{m}_1 's prefer to point up and \mathbf{m}_2 's prefer to point down. Differently, for a positive external field and a negative current, \mathbf{m}_1 's tend to point down, whereas \mathbf{m}_2 's do the opposite. This scenario reveals that the switching is anticlockwise for positive H_y considering that M_1 is stronger than M_2 in the present structure as Fig. 3(d) depicts. The situation differs dramatically when a negative external field (e.g., $H_y = -1000$ Oe) is used; the current-induced magnetization switching is clockwise. This indicates that the switching symmetry is inconsistent with the experimental results shown in Fig 2(a). Moreover, as Fig. 3(d) shows, M_z exhibits opposite nonlinear behavior before switching. Thus, the opposite nonlinear behavior of the Hall resistance before

switching in Fig. 2(b) is well replicated by simulation and can be ascribed to the opposite switching of the upper and lower CoFeBs and their combination. What is more, as expected with the increase in H_y from 250 to 1500 Oe, critical τ for magnetization switching is reduced greatly as displayed in Fig. 3(e), indicating that the critical current density decreases linearly within this range of H_y .

The dynamic evolution of the magnetic moment of the present CoFeB/Ta/CoFeB structure with PMA and antiferromagnetic coupling can be described by performing a macrospin simulation on the basis of the LLG equation,

$$\frac{d\hat{\mathbf{m}}}{dt} = -\gamma\hat{\mathbf{m}} \times \mathbf{H}_{\text{eff}} + \alpha\hat{\mathbf{m}} \times \frac{d\hat{\mathbf{m}}}{dt} + \gamma\zeta_{\parallel}\hat{\mathbf{m}} \times (\hat{\mathbf{m}} \times \hat{\sigma}) + \gamma\zeta_{\perp}\hat{\mathbf{m}} \times \hat{\sigma}, \quad (5)$$

where $\hat{\mathbf{m}}$ represents the unit magnetization moment vector and its orientation is defined in spherical coordinates as depicted in Fig. 4(a), $\hat{\sigma}$ is the spin polarization collinear to the x axis given that we assume the current is along the y direction, γ is gyromagnetic ratio, and α is the damping constant. The effective field \mathbf{H}_{eff} , which has two orthogonal components along polar angle direction H_{θ} and azimuth angle direction H_{φ} , is composed of an external field, an anisotropy field, and an antiferromagnetic coupling effective field. It can be derived from the free energy of our system (see Appendix B). The dampinglike torque coefficient is described by $\zeta_{\parallel} = \frac{\hbar c_{\parallel} J_e}{2eM_s t_F}$, where c_{\parallel} is the dampinglike torque efficiency, J_e is the current density, M_s is the saturation magnetization per unit volume, and t_F denotes the thickness of the ferromagnetic layer. $\zeta_{\perp} = \frac{\hbar c_{\perp} J_e}{2eM_s t_F}$ is the fieldlike torque coefficient, and the fieldlike torque efficiency is represented by c_{\perp} . To make the LLG equation more convenient for calculation, \mathbf{H}_{eff} is normalized by the anisotropy effective field of FM₂, $H_{\text{an}2}$ (more details are presented in Appendix B). Therefore, the LLG equations for the upper FM₁ and lower FM₂ take the dimensionless form of

$$\begin{aligned} \frac{d\hat{\mathbf{m}}_1}{dt} &= -\hat{\mathbf{m}}_1 \times \frac{\mathbf{h}_{\text{eff}1}}{g} + \alpha\hat{\mathbf{m}}_1 \times \frac{d\hat{\mathbf{m}}_1}{dt} \\ &\quad + C_{\parallel} \frac{1}{g} \hat{\mathbf{m}}_1 \times (\hat{\mathbf{m}}_1 \times \hat{\sigma}) + C_{\perp} \frac{1}{g} \hat{\mathbf{m}}_1 \times \hat{\sigma}, \\ \frac{d\hat{\mathbf{m}}_2}{dt} &= -\hat{\mathbf{m}}_2 \times \frac{\mathbf{h}_{\text{eff}2}}{g} + \alpha\hat{\mathbf{m}}_2 \times \frac{d\hat{\mathbf{m}}_2}{dt} \\ &\quad - C_{\parallel} \frac{1}{g} \hat{\mathbf{m}}_2 \times (\hat{\mathbf{m}}_2 \times \hat{\sigma}) - C_{\perp} \frac{1}{g} \hat{\mathbf{m}}_2 \times \hat{\sigma}, \end{aligned} \quad (6)$$

where $\frac{1}{g} = \frac{\gamma H_{\text{an}2}}{2}$ and the normalized torque coefficients are $C_{\parallel} = \gamma\zeta_{\parallel}g = \frac{\hbar c_{\parallel} J_e}{eM_s t_F H_{\text{an}2}}$ and $C_{\perp} = \gamma\zeta_{\perp}g = \frac{\hbar c_{\perp} J_e}{eM_s t_F H_{\text{an}2}}$. For simplicity, the upper FM₁ layer is supposed to possess the same anisotropy and saturation magnetization as the lower FM₂ layer, which do not influence the main results of this simulation. First, the initial positions of \mathbf{m}_1 and \mathbf{m}_2 are set to ensure that they are nearly antiparallel and have a little tilt angle off the z axis. Parameters $M_s = 1300 \text{ emu/cm}^3$, $t_F = 10^{-7} \text{ cm}$, $H_{\text{an}2} = 1333.33 \text{ Oe}$, and $\alpha = 0.01$ were brought into Eq. (6). As a result, magnetization switching trajectories under three typical values of normalized torque coefficient [$C_{\parallel} = 0.75$, $C_{\perp} = 0.4$; $C_{\parallel} = 1.5$, $C_{\perp} = 0.8$; and $C_{\parallel} = 3$, $C_{\perp} = 1.6$ for Figs. 4(b)–4(d), respectively]

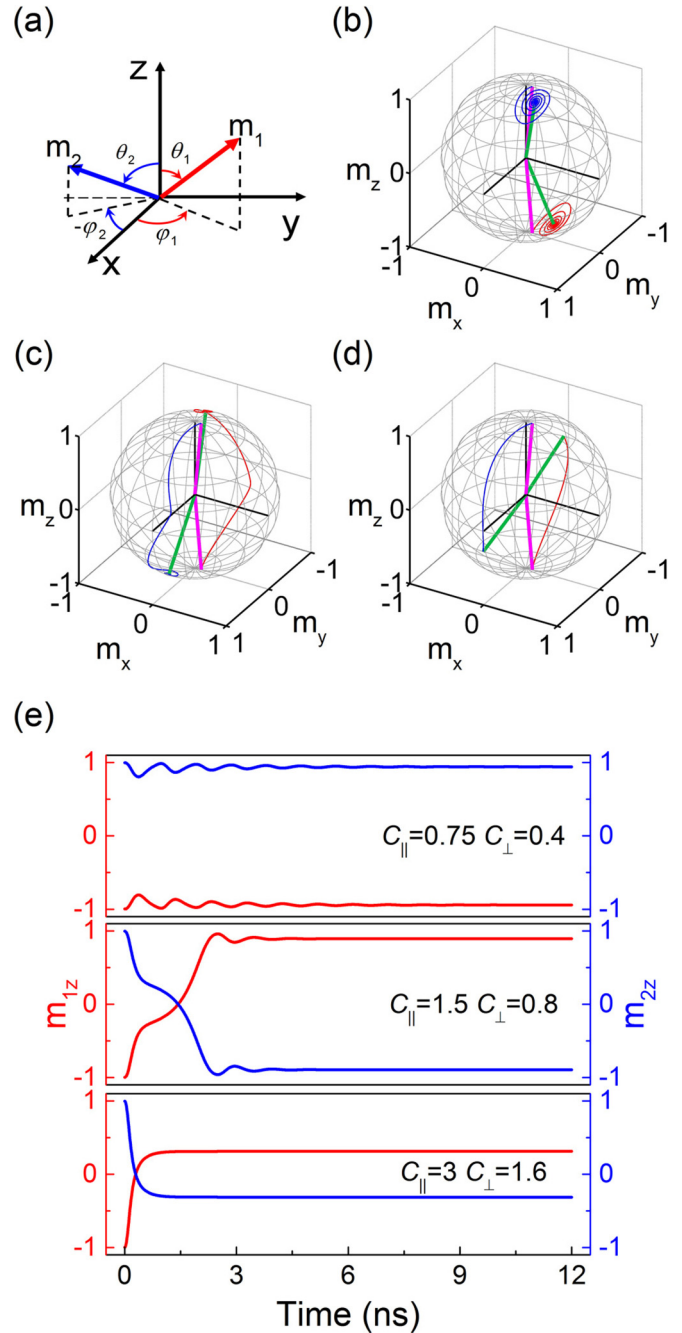


FIG. 4. (a) Orientation of magnetic moments \mathbf{m}_1 and \mathbf{m}_2 defined in the macrospin calculation. Magnetization switching trajectories with the same assistant external field $h_y = 0.375$, antiferromagnetic coupling $a = 2$, and different dimensionless torque coefficients (b) $C_{\parallel} = 0.75$, $C_{\perp} = 0.4$; (c) $C_{\parallel} = 1.5$, $C_{\perp} = 0.8$; and (d) $C_{\parallel} = 3$, $C_{\perp} = 1.6$. The pink solid line and the green solid line represent the initial and final positions of magnetization, respectively. The red curves and the blue curves individually stand for the tracks of magnetic moments \mathbf{m}_1 and \mathbf{m}_2 . (e) Time evolution of the z component of magnetization extracted from (b)–(d).

were calculated with a fixed assistant external field and antiferromagnetic coupling, corresponding to three typical quantities of current density. As depicted in Fig. 4(b), when the dampinglike torque and fieldlike torque coefficients are

0.75 and 0.4, respectively, the magnetic moments \mathbf{m}_1 and \mathbf{m}_2 precess around the final positions near the initial positions, indicating that magnetization switching does not take place under this torque coefficient value. With the dampinglike torque and fieldlike torque coefficients separately increasing up to 1.5 and 0.8, the magnetic moments \mathbf{m}_1 and \mathbf{m}_2 quickly rotate to the opposite hemisphere and then precess around the final equilibrium positions as shown in Fig. 4(c). Figure 4(d) shows that when C_{\parallel} and C_{\perp} rise up to 3 and 1.6, both magnetic moments switch to the opposite hemisphere and stay at the stable position without apparent precession.

We then turn towards the time-dependent magnetic moments' projection on the z axis. Corresponding data are presented in Fig. 4(e). For $C_{\parallel} = 0.75$ and $C_{\perp} = 0.4$, \mathbf{m}_1 and \mathbf{m}_2 move around the equilibrium positions near the initial positions without magnetization switching. For $C_{\parallel} = 1.5$ and $C_{\perp} = 0.8$, the switching of \mathbf{m}_1 and \mathbf{m}_2 happens simultaneously, which is less than 3 ns, accompanied by a relatively long precession around the final states. When C_{\parallel} is up to 3 and C_{\perp} is up to 1.6, \mathbf{m}_1 and \mathbf{m}_2 rapidly switch up and down to the final states. It is worth pointing out that the z components of \mathbf{m}_1 and \mathbf{m}_2 exhibit the same amount of about 0.31 but with opposite signs. This indicates that, if the torque coefficient is large enough, the z components of \mathbf{m}_1 and \mathbf{m}_2 would decrease. As a consequence, the Hall resistance would reduce at a certain amount of applied current density, which is observed in Fig. 2.

IV. SUMMARY

In conclusion, through the spin-orbit torque experiments in MgO/CoFeB/Ta/CoFeB/MgO symmetric heterostructures with PMA and antiferromagnetic coupling, we demonstrate that the spin current generated by the spin Hall effect of Ta diffuses up and down to adjacent CoFeB layers and the magnetization of two CoFeB layers can be switched between two antiparallel states with a critical current density of $\sim 10^7$ A/cm². The experimental results can be well reproduced by simulation. Our findings on spin-orbit torque in the antiferromagnetic coupling system might advance the magnetic memories with low stray fields and low power consumption [33].

Note added. Recently, we found two relevant works reporting spin-orbit torque in synthetic antiferromagnets [34,35].

ACKNOWLEDGMENTS

This work was supported by the National Natural Science Foundation of China (Grants No. 51571128, No. 51671110, and No. 51371191) and the Ministry of Science and Technology of the People's Republic of China (Grant No. 2016YFA0203800).

APPENDIX A: DERIVATION OF TORQUE BALANCE EQUATIONS

The torque balance equation means that the total torques exerted on magnetic moments are equal to zero, which includes the external field torque, the perpendicular anisotropy field torque, the antiferromagnetic coupling field torque, and the

spin torque. Then, for the upper ferromagnetic layer FM₁ and lower ferromagnetic layer FM₂, torque balance equations are expressed as

$$\begin{aligned}\boldsymbol{\tau}_{\text{tot}1} &= -\mathbf{M}_1 \times \mathbf{H}_{\text{eff}1} - \boldsymbol{\tau} \\ &= \boldsymbol{\tau}_{\text{ext}1} + \boldsymbol{\tau}_{\text{an}1} + \boldsymbol{\tau}_{\text{coup}1} - \boldsymbol{\tau} = 0, \\ \boldsymbol{\tau}_{\text{tot}2} &= -\mathbf{M}_2 \times \mathbf{H}_{\text{eff}2} + \boldsymbol{\tau} \\ &= \boldsymbol{\tau}_{\text{ext}2} + \boldsymbol{\tau}_{\text{an}2} + \boldsymbol{\tau}_{\text{coup}2} + \boldsymbol{\tau} = 0,\end{aligned}\quad (\text{A1})$$

with an external field being fixed on the y axis, the free energy of the system is given by

$$\begin{aligned}E &= -(H_y M_1 \cos \omega_1 + H_y M_2 \cos \omega_2) + K_1 \cos^2 \omega_1 \\ &\quad + K_2 \cos^2 \omega_2 + A_{12} \cos(\omega_1 - \omega_2),\end{aligned}\quad (\text{A2})$$

and the effective fields for M_1 and M_2 are expressed as

$$\begin{aligned}\mathbf{H}_{\text{eff}1} &= -\mathbf{e}_{\omega} \frac{\partial E}{M_1 \partial \omega_1} \\ &= -\mathbf{e}_{\omega} \left[H_y \sin \omega_1 - 2 \frac{K_1}{M_1} \cos \omega_1 \sin \omega_1 \right. \\ &\quad \left. - \frac{A_{12}}{M_1} \sin(\omega_1 - \omega_2) \right], \\ \mathbf{H}_{\text{eff}2} &= -\mathbf{e}_{\omega} \frac{\partial E}{M_2 \partial \omega_2} \\ &= -\mathbf{e}_{\omega} \left[H_y \sin \omega_2 - 2 \frac{K_2}{M_2} \cos \omega_2 \sin \omega_2 \right. \\ &\quad \left. + \frac{A_{12}}{M_2} \sin(\omega_1 - \omega_2) \right].\end{aligned}\quad (\text{A3})$$

If τ is not large enough, \mathbf{m}_1 and \mathbf{m}_2 can be proven to remain on the yz plane. Under this situation, all torques lie on the x axis, and the torque balance equations take the simple form of

$$\begin{aligned}\tau_{\text{tot}1} &= \mathbf{e}_x \cdot \boldsymbol{\tau}_{\text{tot}1} = -M_1 H_{\text{eff}1} - \tau \\ &= H_y M_1 \sin \omega_1 - 2K_1 \cos \omega_1 \sin \omega_1 \\ &\quad - A_{12} \sin(\omega_1 - \omega_2) - \tau = 0, \\ \tau_{\text{tot}2} &= \mathbf{e}_x \cdot \boldsymbol{\tau}_{\text{tot}2} = -M_2 H_{\text{eff}2} - \tau \\ &= H_y M_2 \sin \omega_2 - 2K_2 \cos \omega_2 \sin \omega_2 \\ &\quad + A_{12} \sin(\omega_1 - \omega_2) + \tau = 0.\end{aligned}\quad (\text{A4})$$

APPENDIX B: DERIVATION OF THE EFFECTIVE FIELD IN THE LLG EQUATION

In the spherical coordinate, the free energy of our system is expressed as

$$\begin{aligned}E &= -H_y M_1 \sin \theta_1 \sin \varphi_1 - H_y M_2 \sin \theta_2 \sin \varphi_2 \\ &\quad + K_1 \sin^2 \theta_1 + K_2 \sin^2 \theta_2 + A_{12} \cos \langle \mathbf{m}_1, \mathbf{m}_2 \rangle,\end{aligned}\quad (\text{B1})$$

where $\cos \langle \mathbf{m}_1, \mathbf{m}_2 \rangle$ means the cosine of the included angle of \mathbf{m}_1 and \mathbf{m}_2 , which can be derived by cosine law,

and writes

$$\cos \langle \mathbf{m}_1, \mathbf{m}_2 \rangle = \sin \theta_1 \cos \varphi_1 \sin \theta_2 \cos \varphi_2 + \sin \theta_1 \sin \varphi_1 \sin \theta_2 \sin \varphi_2 + \cos \theta_1 \cos \theta_2. \quad (\text{B2})$$

Thus, \mathbf{H}_{eff} 's for FM₁ and FM₂ are expressed as

$$\begin{aligned} \mathbf{H}_{\text{eff}1} &= \mathbf{e}_\theta H_{\theta_1} + \mathbf{e}_\varphi H_{\varphi_1}, \\ H_{\theta_1} &= -\frac{\partial E}{M_1 \partial \theta_1} = -\frac{1}{M_1} (-H_y M_1 \cos \theta_1 \sin \varphi_1 + K_1 \sin 2\theta_1 + A_{12} \cos \theta_1 \cos \varphi_1 \sin \theta_2 \cos \varphi_2 \\ &\quad + A_{12} \cos \theta_1 \sin \varphi_1 \sin \theta_2 \sin \varphi_2 - A_{12} \sin \theta_1 \cos \theta_2), \\ H_{\varphi_1} &= -\frac{\partial E}{M_1 \sin \theta_1 \partial \varphi_1} = -\frac{1}{M_1} (-H_y M_1 \cos \varphi_1 - A_{12} \sin \varphi_1 \sin \theta_2 \cos \varphi_2 + A_{12} \cos \varphi_1 \sin \theta_2 \sin \varphi_2), \\ \mathbf{H}_{\text{eff}2} &= \mathbf{e}_\theta H_{\theta_2} + \mathbf{e}_\varphi H_{\varphi_2}, \\ H_{\theta_2} &= -\frac{\partial E}{M_2 \partial \theta_2} = -\frac{1}{M_2} (-H_y M_2 \cos \theta_2 \sin \varphi_2 + K_2 \sin 2\theta_2 + A_{12} \sin \theta_1 \cos \varphi_1 \cos \theta_2 \cos \varphi_2 \\ &\quad + A_{12} \sin \theta_1 \sin \varphi_1 \cos \theta_2 \sin \varphi_2 - A_{12} \cos \theta_1 \sin \theta_2), \\ H_{\varphi_2} &= -\frac{\partial E}{M_2 \sin \theta_2 \partial \varphi_2} = -\frac{1}{M_2} (-H_y M_2 \cos \varphi_2 - A_{12} \sin \theta_1 \cos \varphi_1 \sin \varphi_2 + A_{12} \sin \theta_1 \sin \varphi_1 \cos \varphi_2). \end{aligned} \quad (\text{B3})$$

Taking the different magnetic parameters of two FM layers into account, we normalize \mathbf{H}_{eff} by the anisotropy effective field of FM₂, namely, $H_{\text{an}2}$. Hence,

$$\begin{aligned} \mathbf{h}_{\text{eff}1} &= \mathbf{e}_\theta h_{\theta_1} + \mathbf{e}_\varphi h_{\varphi_1}, \\ h_{\theta_1} &= \frac{2H_{\theta_1}}{H_{\text{an}2}} = -\frac{1}{m_{12}} (-2h_y m_{12} \cos \theta_1 \sin \varphi_1 + k \sin 2\theta_1 + a \cos \theta_1 \cos \varphi_1 \sin \theta_2 \cos \varphi_2 \\ &\quad + a \cos \theta_1 \sin \varphi_1 \sin \theta_2 \sin \varphi_2 - a \sin \theta_1 \cos \theta_2), \\ h_{\varphi_1} &= \frac{2H_{\varphi_1}}{H_{\text{an}2}} = -\frac{1}{m_{12}} (-2h_y m_{12} \cos \varphi_1 - a \sin \varphi_1 \sin \theta_2 \cos \varphi_2 + a \cos \varphi_1 \sin \theta_2 \sin \varphi_2), \\ \mathbf{h}_{\text{eff}2} &= \mathbf{e}_\theta h_{\theta_2} + \mathbf{e}_\varphi h_{\varphi_2}, \\ h_{\theta_2} &= \frac{2H_{\theta_2}}{H_{\text{an}2}} = 2h_y \cos \theta_2 \sin \varphi_2 - \sin 2\theta_2 - a \sin \theta_1 \cos \varphi_1 \cos \theta_2 \cos \varphi_2 \\ &\quad - a \sin \theta_1 \sin \varphi_1 \cos \theta_2 \sin \varphi_2 + a \cos \theta_1 \sin \theta_2, \\ h_{\varphi_2} &= \frac{2H_{\varphi_2}}{H_{\text{an}2}} = 2h_y \cos \varphi_2 + a \sin \theta_1 \cos \varphi_1 \sin \varphi_2 - a \sin \theta_1 \sin \varphi_1 \cos \varphi_2, \end{aligned} \quad (\text{B4})$$

where $h_y = H_y/H_{\text{an}2}$, $a = \frac{A_{12}}{K_2} (K_2 = \frac{1}{2} H_{\text{an}2} M_2)$, $k = \frac{K_1}{K_2}$, and $m_{12} = \frac{M_1}{M_2}$. Therefore, the LLG equations for the upper FM₁ and lower FM₂ take the form of

$$\begin{aligned} \frac{d\hat{\mathbf{m}}_1}{dt} &= -\hat{\mathbf{m}}_1 \times \frac{\mathbf{h}_{\text{eff}1}}{g} + \alpha \hat{\mathbf{m}}_1 \times \frac{d\hat{\mathbf{m}}_1}{dt} + C_{\parallel} \frac{1}{g} \hat{\mathbf{m}}_1 \times (\hat{\mathbf{m}}_1 \times \hat{\boldsymbol{\sigma}}) + C_{\perp} \frac{1}{g} \hat{\mathbf{m}}_1 \times \hat{\boldsymbol{\sigma}}, \\ \frac{d\hat{\mathbf{m}}_2}{dt} &= -\hat{\mathbf{m}}_2 \times \frac{\mathbf{h}_{\text{eff}2}}{g} + \alpha \hat{\mathbf{m}}_2 \times \frac{d\hat{\mathbf{m}}_2}{dt} - C_{\parallel} \frac{1}{g} \hat{\mathbf{m}}_2 \times (\hat{\mathbf{m}}_2 \times \hat{\boldsymbol{\sigma}}) - C_{\perp} \frac{1}{g} \hat{\mathbf{m}}_2 \times \hat{\boldsymbol{\sigma}}, \end{aligned} \quad (\text{B5})$$

where $\frac{1}{g} = \frac{\gamma H_{\text{an}2}}{2}$ and the normalized dampinglike torque coefficient is $C_{\parallel} = \gamma \zeta_{\parallel} g = \frac{\hbar c_{\parallel} J_c}{e M_s t_F H_{\text{an}2}}$ and the fieldlike torque coefficient is $C_{\perp} = \gamma \zeta_{\perp} g = \frac{\hbar c_{\perp} J_c}{e M_s t_F H_{\text{an}2}}$.

-
- [1] J. E. Hirsch, *Phys. Rev. Lett.* **83**, 1834 (1999).
[2] S. F. Zhang, *Phys. Rev. Lett.* **85**, 393 (2000).
[3] Y. K. Kato, R. C. Myers, A. C. Gossard, and D. D. Awschalom, *Science* **306**, 1910 (2004).
[4] S. O. Valenzuela and M. Tinkham, *Nature (London)* **442**, 176 (2006).
[5] M. Ehlert, C. Song, M. Ciorga, M. Utz, D. Schuh, D. Bougeard, and D. Weiss, *Phys. Rev. B* **86**, 205204 (2012).
[6] W. Zhang, W. Han, X. Jiang, S.-H. Yang, and S. S. P. Parkin, *Nat. Phys.* **11**, 496 (2015).
[7] C. H. Du, H. L. Wang, F. Y. Yang, and P. C. Hammel, *Phys. Rev. B* **90**, 140407(R) (2014).
[8] H. L. Wang, C. H. Du, Y. Pu, R. Adur, P. C. Hammel, and F. Y. Yang, *Phys. Rev. Lett.* **112**, 197201 (2014).
[9] L. Liu, C. F. Pai, Y. Li, H. W. Tseng, D. C. Ralph, and R. A. Buhrman, *Science* **336**, 555 (2012).

- [10] L. Liu, O. J. Lee, T. J. Gudmundsen, D. C. Ralph, and R. A. Buhrman, *Phys. Rev. Lett.* **109**, 096602 (2012).
- [11] J. Kim, J. Sinha, M. Hayashi, M. Yamanouchi, S. Fukami, T. Suzuki, S. Mitani, and H. Ohno, *Nature Mater.* **12**, 240 (2013).
- [12] D. Bhowmik, L. You, and S. Salahuddin, *Nat. Nanotechnol.* **9**, 59 (2014).
- [13] H. Reichlová, D. Kriegner, V. Holý, K. Olejník, V. Novák, M. Yamada, K. Miura, S. Ogawa, H. Takahashi, T. Jungwirth, and J. Wunderlich, *Phys. Rev. B* **92**, 165424 (2015).
- [14] M. Akyol, G. Yu, J. G. Alzate, P. Upadhyaya, X. Li, K. L. Wong, A. Ekicibil, P. K. Amiri, and K. L. Wang, *Appl. Phys. Lett.* **106**, 162409 (2015).
- [15] S. Fukami, C. Zhang, S. DuttaGupta, A. Kurenkov, and H. Ohno, *Nature Mater.* **15**, 535 (2016).
- [16] Y.-C. Lau, D. Betto, K. Rode, J. M. D. Coey, and P. Stamenov, *Nat. Nanotechnol.* **11**, 758 (2016).
- [17] Y.-W. Oh, S. C. Baek, Y. M. Kim, H. Y. Lee, K.-D. Lee, C.-G. Yang, E.-S. Park, K.-S. Lee, K.-W. Kim, G. Go, J.-R. Jeong, B.-C. Min, H.-W. Lee, K.-J. Lee, and B.-G. Park, *Nat. Nanotechnol.* **11**, 878 (2016).
- [18] Y. Yan, C. Wan, X. Zhou, G. Shi, B. Cui, J. Han, Y. Fan, X. Han, K. L. Wang, F. Pan, and C. Song, *Adv. Electron. Mater.* **2**, 1600219 (2016).
- [19] X. Zhang, C. H. Wan, Z. H. Yuan, Q. T. Zhang, H. Wu, L. Huang, W. J. Kong, C. Fang, U. Khan, and X. F. Han, *Phys. Rev. B* **94**, 174434 (2016).
- [20] S. Emori, U. Bauer, S.-M. Ahn, E. Martinez, and G. S. D. Beach, *Nature Mater.* **12**, 611 (2013).
- [21] D. Bang, J. Yu, X. Qiu, Y. Wang, H. Awano, A. Manchon, and H. Yang, *Phys. Rev. B* **93**, 174424 (2016).
- [22] K. Garello, I. M. Miron, C. O. Avci, F. Freimuth, Y. Mokrousov, S. Blugel, S. Auffret, O. Boulle, G. Gaudin, and P. Gambardella, *Nat. Nanotechnol.* **8**, 587 (2013).
- [23] X. Fan, J. Wu, Y. Chen, M. J. Jerry, H. Zhang, and J. Q. Xiao, *Nat. Commun.* **4**, 1799 (2013).
- [24] P. M. Haney, H.-W. Lee, K.-J. Lee, A. Manchon, and M. D. Stiles, *Phys. Rev. B* **87**, 174411 (2013).
- [25] H. V. Gomonay and V. M. Loktev, *Phys. Rev. B* **81**, 144427 (2010).
- [26] O. V. Gomonay and V. M. Loktev, *Low Temp. Phys.* **41**, 698 (2015).
- [27] P. Wadley, B. Howells, J. Železný, C. Andrews, V. Hills, R. P. Campion, V. Novák, K. Olejník, F. Maccherozzi, S. S. Dhesi, S. Y. Martin, T. Wagner, J. Wunderlich, F. Freimuth, Y. Mokrousov, J. Kuneš, J. S. Chauhan, M. J. Grzybowski, A. W. Rushforth, K. W. Edmonds, B. L. Gallagher, and T. Jungwirth, *Science* **351**, 587 (2016).
- [28] S. Woo, M. Mann, A. J. Tan, L. Caretta, and G. S. D. Beach, *Appl. Phys. Lett.* **105**, 212404 (2014).
- [29] P. Grunberg, R. Schreiber, Y. Pang, M. B. Brodsky, and H. Sowers, *Phys. Rev. Lett.* **57**, 2442 (1986).
- [30] S. S. P. Parkin, *Phys. Rev. Lett.* **67**, 3598 (1991).
- [31] X. Zhang, Y. Zhang, and J. W. Cai, *J. Appl. Phys.* **118**, 143903 (2015).
- [32] C. Tannous and J. Gieraltowski, *Eur. J. Phys.* **29**, 475 (2008).
- [33] Y. Wang, X. Zhou, C. Song, Y. Yan, S. Zhou, G. Wang, C. Chen, F. Zeng, and F. Pan, *Adv. Mater.* **27**, 3196 (2015).
- [34] C. Bi, H. Almasi, K. Price, T. Newhouse-Illige, M. Xu, S. R. Allen, X. Fan, and W. Wang, *Phys. Rev. B* **95**, 104434 (2017).
- [35] V. Risinggård and J. Linder, [arXiv:1701.00786](https://arxiv.org/abs/1701.00786).